Reactive Deposition of Conformal Metal Oxide Films from Supercritical Carbon Dioxide

Adam O'Neil and James J. Watkins*

Polymer Science and Engineering Department, University of Massachusetts, Amherst, Massachusetts 01003

Received January 30, 2007. Revised Manuscript Received September 4, 2007

High-purity conformal metal oxide films were deposited onto planar and etched silicon wafers by surface-selective precursor hydrolysis in supercritical carbon dioxide using a cold wall reactor. Continuous films of cerium, hafnium, titanium, niobium, tantalum, zirconium, and bismuth oxides between 21 and 263 nm thick were grown at temperatures between 250 and 300 °C using CO_2 soluble precursors. The as-deposited films were pure single-phase oxide in the cases of HfO_2, ZrO_2, and TiO_2 and composed of oxides of mixed oxidation states in the cases of cerium, tantalum, niobium, and bismuth oxides as determined by XPS. As-deposited films typically contained 5% carbon or less. Carbon contamination was eliminated in all cases by annealing at 400 °C. The films were characterized by XPS, profilometry, SEM, XRD, and AFM.

Introduction

Metal oxide films are of great interest for a diverse array of applications that rely on their chemical, electrical, and magnetic properties.[1] Examples include gate oxides,[2] capacitors,[3] ferroelectrics,[4] membranes,[5] catalyst supports,[6] thermoelectrics,[7] and superconductors.[8] Conventional techniques for generating films include chemical vapor deposition (CVD) and atomic layer deposition (ALD); however, both are subject to specific limitations.[9−12] CVD typically requires the use of oxidants such as O_2 or O_3 and temperatures in excess of 400 °C, which can limit the applicability of this approach for many microelectronic applications. Conformal deposition within high aspect ratio device features using CVD can also be problematic due to poor step coverage, which often has origins in low vapor-phase precursor concentrations due to limited precursor volatility. ALD provides excellent step coverage via deposition of submonolayer quantities of oxide in each reaction cycle. The number of reactive cycles required to generate films thicker than a few nanometers and the associated process time, however, is an issue for many applications that require thicker films. Moreover, like CVD precursors, ALD precursors are subject to volatility constraints. Finally, ALD often employs metal chlorides as precursors, which can lead to chlorine contamination in the final film. Here, we demonstrate a new technique for the generation of conformal metal oxide films including cerium, hafnium, titanium, niobium, tantalum, zirconium, and bismuth oxides via precursor hydrolysis in supercritical carbon dioxide followed by annealing.

Supercritical fluid deposition (SFD) is a well-established technique for the reactive deposition of pure, conformal metal films, typically under reducing conditions. We and others have demonstrated the deposition of copper, cobalt, nickel, platinum, ruthenium, palladium, gold, rhodium, and iridium films.[13−21] Alloys can be deposited using mixed precursor systems[22] and metal films can be doped with inorganic species using a similar approach. For example, phosphorus-doped cobalt films have been deposited using tris(2,2,6,6-tetramethylheptane-3,5-dionato)cobalt and triphenylphosphine.[23]

(1) Dagotto, E. *Science* **2005**, *309*, 257−262.
(2) Pan, T. M.; Chien, C. H.; Lei, T. F.; Chao, T. S.; Huang, T. Y. *Electrochem. Solid State Lett.* **2001**, *4*, F15−F17.
(3) Kukli, K.; Ritala, M.; Markku Leskela, M. *J. Electrochem. Soc.* **2001**, *148*, F35−F41.
(4) Ramesh, R.; Luther, K. B.; Wilkens, B.; Hart, D. L.; Wang, E.; Tarascon, J. M.; Inam, A.; Wu, X. D.; Venkatesan, T. *Appl. Phys. Lett.* **1990**, *57*, 1505−1507.
(5) Oishi, N.; Atkinson, A.; Brandon, N. P.; Kilner, J. A.; Steele, B. C. H. *J. Am. Ceram. Soc.* **2005**, *88*, 1394−1396.
(6) Trovarelli, A. *Catal. Rev.-Sci. Eng.* **1996**, *38*, 439−520.
(7) Kuomoto, K.; Terasaki, I.; Funahashi, R. *MRS Bull.* **2006**, *31*, 206−210.
(8) Tokura, Y.; Takagi, H.; Uchida, S. *Nature* **1989**, *337*, 345−347.
(9) Barreca, D.; Gasparotto, A.; Tondello, E.; Sada, C.; Polizzi, S.; Benedetti, A. *Chem. Vap. Deposition* **2003**, *9*, 199−206.
(10) Becht, M.; Morishita, T. *Chem. Vap. Deposition* **1996**, *2*, 191−197.
(11) Paivasaari, J.; Putkonen, M.; Niinisto, L. *J. Mater. Chem.* **2002**, *12*, 1828−1832.
(12) Edleman, N. L.; Wang, A. C.; Belot, J. A.; Metz, A. W.; Babcock, J. R.; Kawaoka, A. M.; Ni, J.; Metz, M. V.; Flaschenriem, C. J.; Stern, C. L.; Liable-Sands, L. M.; Rheingold, A. L.; Markworth, P. R.; Chang, R. P. H.; Chudzik, M. P.; Kannewurf, C. R.; Marks, T. J. *Inorg. Chem.* **2002**, *41*, 5005−5023.
(13) Blackburn, J. M.; Long, D. P.; Cabanas, A.; Watkins, J. J. *Science* **2001**, *294*, 141−145.
(14) Cabanas, A.; Long, D. P.; Watkins, J. J. *Chem. Mater.* **2004**, *16*, 2028−2033.
(15) Cabanas, A.; Blackburn, J. M.; Watkins, J. J. *Microelectron. Eng.* **2002**, *64*, 53−61.
(16) O'Neil, A.; Watkins, J. J. *Chem. Mater.* **2006**, *18*, 5652−5658.
(17) Hunde, E. T.; Watkins, J. J. *Chem. Mater.* **2004**, *16*, 498−503.
(18) Kondoh, E.; Kato, H. *Microelectron. Eng.* **2002**, *64*, 495−499.
(19) Kondoh, E. *Jpn. J. Appl. Phys., Part 1* **2004**, *43*, 3928−3933.
(20) Ye, X. R.; Wai, C. M.; Zhang, D. Q.; Kranov, Y.; McIlroy, D. N.; Lin, Y. H.; Engelhard, M. *Chem. Mater.* **2003**, *15*, 83−91.
(21) Zhao, B.; Momose, T.; Shimogaki, Y. *Jpn. J. Appl. Phys., Part 1* **2006**, *45*, L1296−L1299.
(22) Watkins, J. J.; McCarthy, T. J. U.S. Patent 5,789,027, 1998.
(23) Blackburn, J. M.; Gaynor, J.; Drewery, J.; Hunde, E.; Watkins, J. J. *Advanced Metallization Conference Proceedings*; Materials Research Society: Warrendale, PA, 2003; pp 601−605.

10.1021/cm070288s CCC: $37.00 © 2007 American Chemical Society
Published on Web 10/24/2007

Table 1. Representative Results for Metal Oxide Deposition from Supercritical CO_2[a]

expt.	precursor	purge temp (°C)	purge time (h)	CO_2 dried	water added (μL)	deposition temp (°C)	average film thickness (nm)	film color
1	$Ce(tmhd)_4$	150	15	no	0	250	58	gray
2	$Ce(tmhd)_4$	150	15	yes	0	250	21	gray
3	$Ce(tmhd)_4$	150	15	yes	2	250	216	light blue
4	$Ce(tmhd)_4$	150	15	yes	5	250	247	purple
5	$Ce(tmhd)_4$	150	15	yes	10	250	263	purple
5	$Ce(tmhd)_4$	150	15	yes	10	250	250	purple
6	$Ce(tmhd)_4$	150	15	yes	15	250	243	purple
7	$Hf(tmhd)_4$	150	15	yes	10	300	127	gray blue
8	$Zr(tmhd)_4$	150	15	yes	15	300	85	light blue
9	$Ta(OEt)_4(acac)$	60	1	no	0	300	78	gray
10	$Nb(tmhd)_4$	60	1	yes	5	300	98	blue
11	$Ti(tmhd)_2(i\text{OPr})_2$	60	1	no	0	300	154	blue
12	$Bi(Ph)_3$	60	1	no	0	350	64	light blue

[a] Reaction pressures varied between 20 and 25 MPa in a high-pressure cold wall reactor.

Supercritical fluids (SCFs) offer enabling advantages for reactive depositions by providing a unique environment that allows solution-based chemistry in a media with transport properties approaching those of a gas, including high diffusivities and the absence of surface tension. Because precursors are transported in SCF solution, 1000-fold increases in precursor concentration compared to vapor-phase depositions can readily be realized.[24] High precursor concentration mitigates mass-transport limitations to conformal film depositions and promotes surface reaction-rate-limited kinetics to provide exceptional step coverage. We have validated this conclusion directly for Cu and Ru through kinetic studies that indicate zero-order deposition kinetics with respect to precursor concentration.[24]

Investigations of the use of SCFs for metal oxide deposition were previously conducted by Hansen et al. who employed rapid expansion of SCF solutions of precursors to create aerosols that were sprayed onto a heated target substrate and pyrolized at ambient pressure to yield metal oxide and mixed oxide systems, including complex superconducting oxides.[25] Uchida et al. demonstrated direct growth of TiO_2 films by spraying supercritical precursor solution directly onto a substrate heated to 80−120 °C.[26] Recently, Gougousi et al. demonstrated that a suitable oxidizing agent, such as hydrogen peroxide or *tert*-butyl peracetate enabled low-temperature deposition of planar Al_2O_3, ZrO_2, MnO_x, and RuO_x films in carbon dioxide.[27]

Here, we report the extension of our surface-selective, cold wall, SCF metal deposition process to yield conformal pure metal oxide films. Cerium, hafnium, titanium, niobium, tantalum, zirconium, and bismuth oxide films were deposited from organometallic compounds in CO_2 by reaction of the precursor with water present in the CO_2, either added in controlled amounts or present as an impurity in the system. Drying CO_2 to remove adventitious water prior to the deposition resulted in suppression of film growth. The deposited films ranged in thickness from 21 to 263 nm depending on precursor, precursor reactivity, water concentration, and reaction conditions. Films were characterized by XPS, SEM, AFM, XRD, and profilometry.

(24) Zong, Y. F.; Watkins, J. J. *Chem. Mater.* **2005**, *17*, 560−565.
(25) Hansen, B. N.; Hybertson, B. M.; Barkley, R. M.; Sievers, R. E. *Chem. Mater.* **1992**, *4*, 749−752.
(26) Uchida, H.; Otsubo, A.; Itatani, K.; Koda, S. *Jpn. J. Appl. Phys., Part 1* **2005**, *44*, 1901−1906.
(27) Gougousi, T.; Barua, D.; Young, E. D.; Parsons, G. N. *Chem. Mater.* **2005**, *17*, 5093−5100.

Experimental Section

Tetrakis(2,2,6,6-tetramethyl-3,5-heptanedionato) hafnium ($Hf(tmhd)_4$), titanium bis(2,2,6,6-tetramethyl-3,5-heptanedionato) diisopropoxide ($Ti(tmhd)_2(i\text{OPr})_2$), and triphenyl bismuth ($Bi(Ph)_3$) were obtained from Gelest. Tetrakis(2,2,6,6-tetramethyl-3,5-heptanedionato) cerium ($Ce(tmhd)_4$), tetraethoxy acetylacetanato tantalum ($Ta(OEt)_4(acac)$, tetrakis(2,2,6,6-tetramethyl-3,5-heptanedionato) zirconium ($Zr(tmhd)_4$), and tetrakis(2,2,6,6-tetramethyl-3,5-heptanedionato) niobium ($Nb(tmhd)_4$) were obtained from Strem Chemicals. β-Diketonate-based metal complexes were found to be a generally useful class of precursor due to their high thermal stability and acceptable solubility in supercritical carbon dioxide. Coleman-grade CO_2 (99.99%) was obtained from Merriam Graves. Water concentration for the Coleman grade is reported to be <10 ppm. Dry nitrogen was supplied in house from a liquid source. Planar silicon (100) wafers (2 in.) were used directly. Etched wafers were either thermally grown silica (via) or IBM 185 silicon nitride (trench) and were cut to 25 × 20 mm pieces prior to deposition.

The depositions were performed in a cold wall vessel with an internal volume of 80 mL. Sample wafers were mounted on a heated stage within the vessel. Solid precursor (0.1 mmol) (0.14−2.8 wt % in CO_2 at the deposition conditions) was added to the vessel prior to sealing. The system was purged with N_2 at 60 or 150 °C prior to CO_2 addition. CO_2 (11−20 MPa) was delivered to the reactor using a 500 mL ISCO syringe pump. When dried CO_2 was required, the gas was passed through a 160 mL column packed with 4 Å molecular sieves. For experiments using controlled addition of water, known volumes of water were added to the flow of CO_2 after the drying column using a Valco 6 port valve equipped with 2, 5, 10, or 15 μL sample loops. The experiments were conducted in simple batch mode. In all cases the precursor was dissolved in CO_2 over 60 min prior to initiating deposition by heating the stage. Higher soak temperatures (e.g., 150 °C) improved the dissolution rate of some precursors including ($Ce(tmhd)_4$, $Hf(tmhd)_4$, $Zr(tmhd)_4$, and $Bi(Ph)_3$); however, the modest thermal stability of $Ti(tmhd)_2(i\text{OPr})_2$, $Nb(tmhd)_4$, and $Ta(OEt)_4(acac)$ required the use of lower soak temperatures (60 °C). Following precursor dissolution, the stage was heated to the desired reaction temperature. Films were deposited over a temperature range of 100−350 °C, but most depositions, including those reported in Table 1, were conducted between 250 and 300 °C. Depositions at

lower temperatures often resulted in extensive carbon contamination. The reaction start time was taken as the time at which the stage was within 5 °C of the setpoint. The temperature was maintained at the setpoint for 30 min for each deposition. After 30 min the power was cut to the pedestal heater and the stage temperature dropped below 200 °C rapidly, effectively terminating the deposition. Wafer annealing, when applicable, was performed in air at 400 °C for 1 h to remove carbon and at 800 °C over 1 h and 6 h periods to initiate film crystallization.

The deposited films were analyzed by X-ray photoelectron spectroscopy (XPS) using a Quantum 2000 Scanning ESCA Microprobe (Physical Electronics) equipped with an Ar^+ ion-sputtering gun and charge neutralizing system. Data were analyzed using Multipak software (version 6.1, Physical Electronics). Film thicknesses were measured by profilometry using a Dektak 3 profilometer. XRD analysis was performed with a Panalytical X-PERT diffractometer. XRD peak indexing was carried out using DICVOL04 indexing software.[28,29] Surface roughness measurements were made using a National Instruments Dimension 3100 SPM used in contact mode with a SiN tip. SEM images were obtained using a JEOL 6320 field emission microscope. SEM samples were mounted on a cross-cut aluminum stub. Samples were lightly coated with Pt (~3 nm) prior to examination.

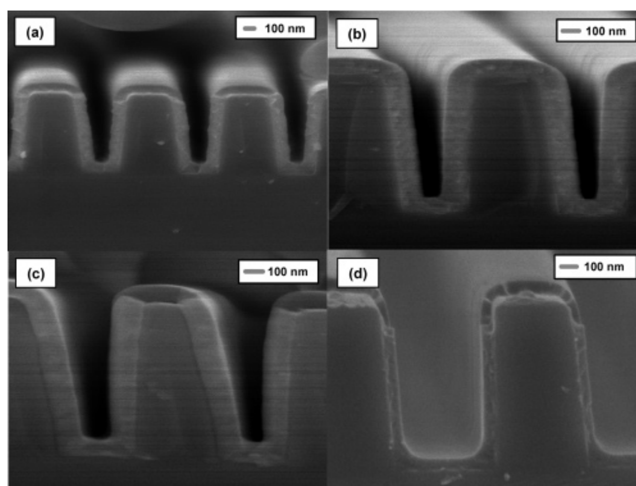

Figure 1. SEM images of films grown on silicon nitride trench structures. Conformal films are grown of hafnium dioxide (a), cerium oxide (b), zirconium oxide (c), and titanium dioxide (d).

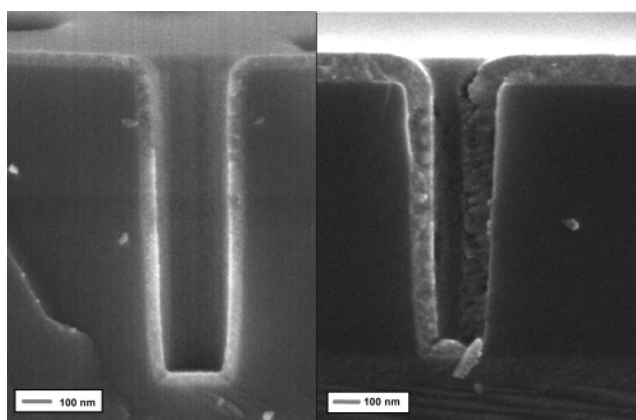

Figure 2. SEM images of via structures indicating conformal coverage of hafnium dioxide (a) and cerium oxide (b).

Results and Discussion

Typical deposition results for cerium, hafnium, titanium, niobium, tantalum, zirconium, and bismuth oxides are summarized in Table 1. The films deposited by SFD were continuous, uniform, and brightly colored. For each oxide, the color variation corresponded to changes in film thickness, as measured by profilometry.

As expected for a hydrolysis mechanism, the presence of adventitious water as well as the controlled addition of water impacted deposition rate and film thickness. For depositions using $Ce(tmhd)_4$, $Hf(tmhd)_4$, and $Zr(tmhd)_4$ the reactor was purged with dry nitrogen at 150 °C for 15 h to remove adsorbed water.[30] In the cases of $Ti(tmhd)_2(iOPr)_2$, $Nb(tmhd)_4$, and $Ta(OEt)_4(acac)$, thermal stability limitations for the precursors required lower purge temperatures (60 °C) and shorter purge times (1 h).

The influence of water concentration on film growth for ceria using $Ce(tmhd)_4$ as precursor is described in Table 1. We find that trace water is present in Coleman-grade CO_2 at sufficient concentrations to yield a thin film via precursor hydrolysis. For example, 30 min depositions at a stage temperature of 250 °C using as-received Coleman-grade CO_2 yielded a 58 nm thick film. The moisture content of the as-received CO_2 was reduced by flow through molecular sieves prior to delivery and deposition. The use of dried CO_2 reduced the deposited film thickness to 21 nm. It is not surprising that this simple drying step did not completely arrest film deposition. The relatively high density of CO_2 at the deposition conditions renders even trace concentrations of water significant relative to the mass of precursor used. For a typical deposition in our 80 mL reactor at a precursor loading of 0.1 mmol, 10 ppm water in CO_2 yields a precursor:water mole ratio of 16:1, sufficient for the deposition of a 25−40 nm film assuming complete conversion and uniform substrate coverage. The influence of water concentration was further examined by the addition of 2 and 5 μL of water to dried CO_2 prior to delivery and deposition, which produced films with thicknesses of 216 and 247 nm, respectively. These additions represent water concentrations in CO_2 of approximately 0.11 and 0.275 mmol, respectively, and molar ratios of precursor:H_2O of approximately 1:1 and 1:3. Further increase in the water concentration did not substantially influence film thickness. At very high water concentration decreases in film thickness were observed. This could be attributed to gas-phase nucleation or possibly a reduction in the solubility of the precursor in the humidified CO_2.

The observations presented above are consistent with a hydrolysis mechanism; however, reaction with adventitious oxygen present in the system should be considered. Coleman-grade CO_2 contains <9 ppm Ar + O_2.[31] We find however that the use of supercritical fluid grade CO_2, which reportedly contains less O_2 (<1 ppm Ar + O_2) does not result in a change in deposition thickness at equivalent conditions. Moreover, at the deposition temperatures employed, molec-

(28) Louer, D.; Louer, M. *J. Appl. Crystallogr.* **1972**, *5*, 271−275.
(29) Boultif, A.; Louer, D. *J. Appl. Crystallogr.* **2004**, *37*, 724−731.
(30) Control experiments indicate that no deposition occurs and less than 1.5% of the precursor was lost to sublimation during the purging step.
(31) *Speciality Gas and Equipment Catalogue*; Merriam-Graves: Charlestown, NH, 2006.

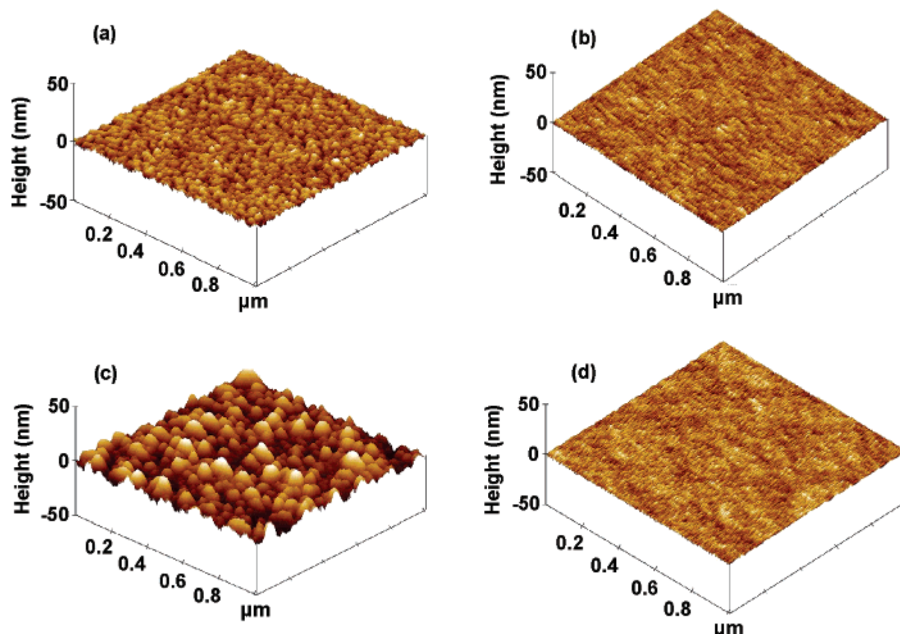

Figure 3. AFM analysis of hafnium oxide and cerium oxide films indicates a significant reduction in surface roughness upon annealing of the as-deposited film. The rms roughness decreases from 1.3 to 0.8 nm following a 400 °C anneal in the case of hafnium dioxide (a, b) and from 3.1 to 0.7 nm for cerium oxide (c, d).

ular oxygen derived precursor oxidation is not expected to be the predominant mechanism. $Ce(tmhd)_4$ is reported to be stable in dry air up to ~300 °C;[32] however, the precursor begins to decompose at ~220 °C in the presence of moisture.[33] In addition, CVD experiments using $Ce(tmhd)_4$ as precursor do not yield oxide films in the presence of oxygen below 400 °C without plasma enhancement.[9] We are currently undertaking a detailed study of metal oxide deposition kinetics via SFD.

SEM analysis of the films deposited onto patterned substrates indicates that SFD yields remarkable step coverage. Figure 1 shows hafnia (a), ceria (b), zirconia (c), and titania (d) films deposited within sub-micrometer trench structures. Examples of hafnia and ceria depositions within 300 nm diameter × 1.2 μm deep SiO_2 via structures are shown in Figure 2. The hafnia and ceria films were analyzed by AFM and typical results are shown in Figure 3. The rms roughness for as-deposited ceria and hafnia films were 3.1 and 1.3 nm, respectively. Following annealing at 400 °C, roughness was reduced to 0.7 and 0.8 nm, respectively.

XPS sputtering profile data and survey spectra for cerium, hafnium, titanium, niobium, tantalum, zirconium, and bismuth oxides are shown in Figure 4 and indicate that high-purity continuous films were deposited in each case. The data indicate that Hf, Zr, and Ti oxides were deposited in the 4+ oxidation states, while Nb, Ta, Bi, and Ce were deposited in mixed oxidation states. Ceria films, Figures 4c and 4d, were essentially carbon-free in the bulk within the detection limits of our instrument at the deposition conditions studied. All films exhibited significant carbon contamination at the surface, as would be expected. High-resolution analysis of the Ce $3d_{5/2}$ (884.0 eV) and $3d_{3/2}$ (902.0 eV) indicated the unannealed ceria films were predominantly Ce^{3+} oxide in the bulk, while the surface layer was comprised of Ce in a mixed oxidation state. The presence of carbonate at the surface is likely. After annealing at 400 °C, the surface was found to be composed predominantly of Ce^{4+}, while the bulk remained as Ce^{3+} oxide (Figures 5g and 5h).

All other oxide films (hafnium, titanium, niobium, tantalum, zirconium, and bismuth oxides) were deposited with less than 5% carbon in the bulk as determined by XPS. In each case, carbon contamination in the films was reduced below the detection limits of the XPS instrument by annealing for 1 h in air at 400 °C. Several low-temperature depositions of titania were carried out for direct comparison of SFD to the spray deposition of Uchida et al.[26] In our experiments, no deposition was observed below 100 °C, and films generally had high carbon contents if grown below 200 °C, typically ~45%. Increasing deposition temperature reduces carbon content to approximately 5%. Figures 4e and 4f show that for a titania film deposited at 300 °C and annealed at 400 °C for 1 h no detectable carbon is present. Bismuth data collected following a 6 h 800 °C anneal are shown in Figure 4o. Bismuth diffusion into the silicon substrate is evident. At the lower anneal temperature of 400 °C, Figures 4m and 4n, diffusion of bismuth into the substrate was not observed.

Sputter depth profiling was used to compare spectra taken close to the surface of the films to spectra acquired after multiple sputtering cycles closer to the Si wafer interface. Tantalum oxide films, Figures 5a and 5b, show peaks at 29.1 eV ($4f_{5/2}$) and 27.2 eV ($4f_{7/2}$) at the surface, indicating Ta^{5+} oxide is the only species present. Within the bulk and closer

(32) *Chemicals for Research*; Strem Chemicals: Newburyport: MA, 2006.
(33) 0.5 g of $Ce(tmhd)_4$ precursor was heated in a sealed vessel purged first with dry nitrogen and then with nitrogen passed through a water-filled bubbler prior to the vessel. Decomposition of cerium precursor was observed by color change from dark brown to straw yellow. Decomposition was observed at 220 °C in the case of humidified nitrogen, while temperatures approaching 300 °C were required for decomposition in dry nitrogen.

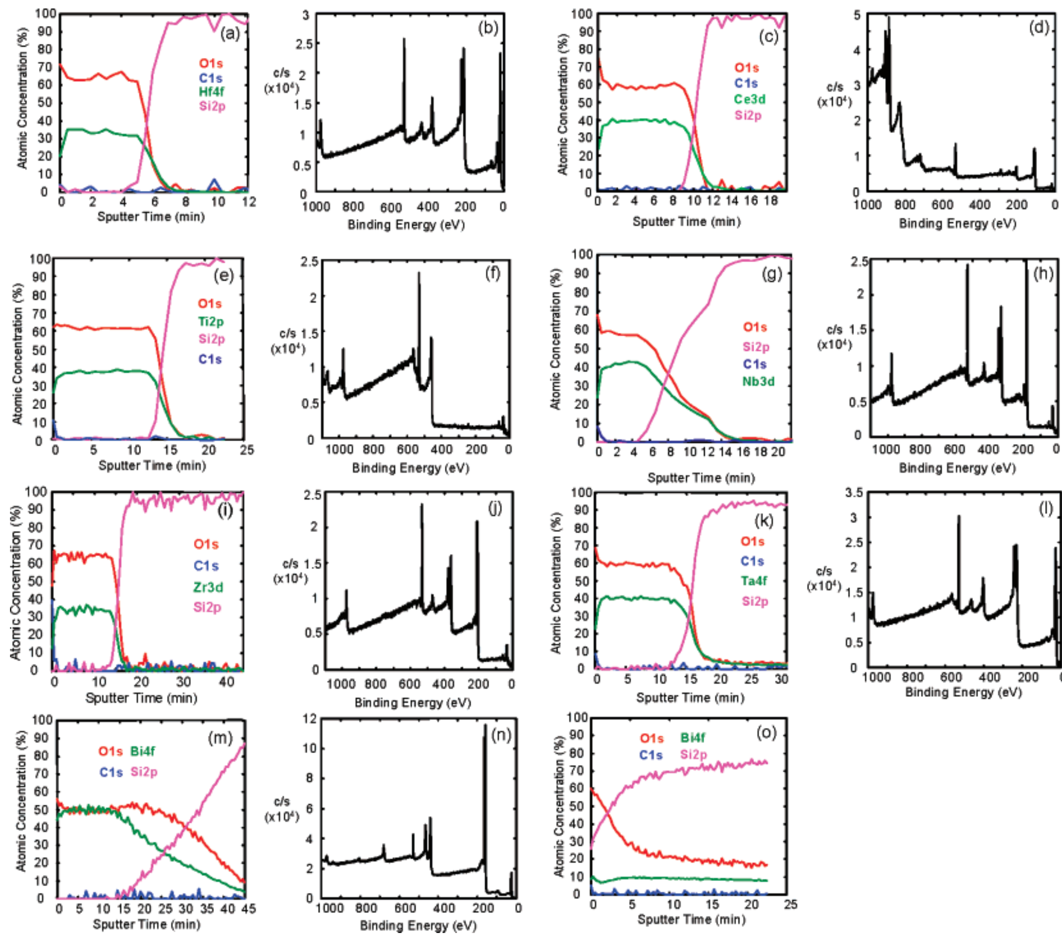

Figure 4. XPS sputter profiles and survey spectra of metal oxide films following a 400 °C anneal; carbon is not observed within the detection limits of the instrument. Peaks in the 200−300 eV region of the ceria and titania spectra are due to Ce 4s and Ar 2p, respectively. The spectra shown are for (a, b) hafnium dioxide, (c, d) cerium oxide, (e, f) titanium dioxide, (g, h) niobium oxide, (i, j) zirconium dioxide, (k, l) tantalum oxide, and (m, n) bismuth oxide. Image (o) shows results for the bismuth oxide film following an 800 °C anneal, for which the diffusion of Bi into the underlying silicon substrate is observed.

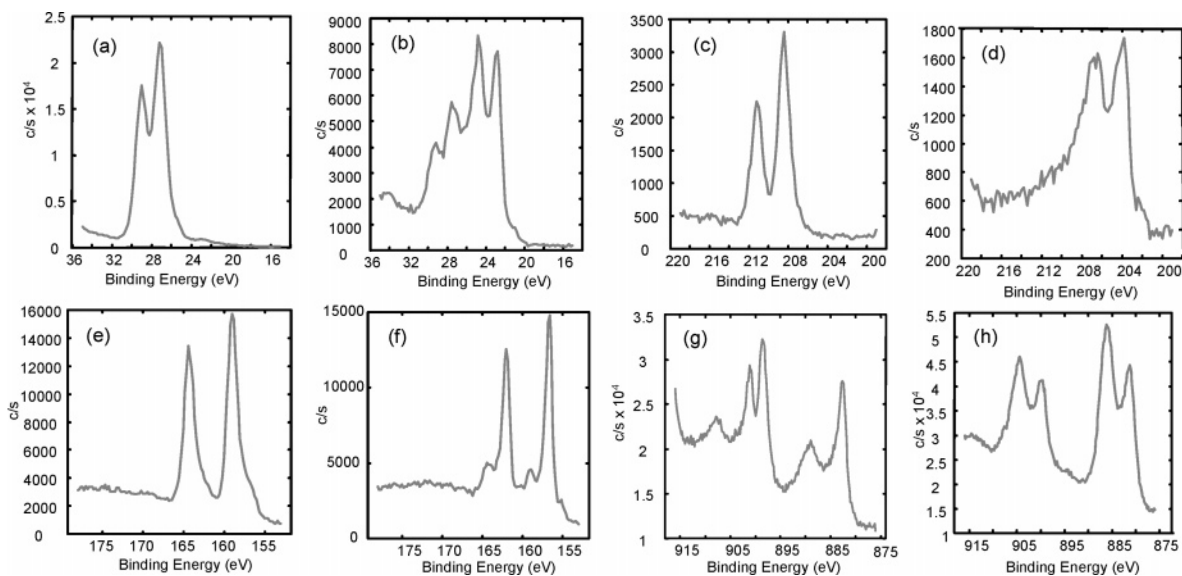

Figure 5. XPS spectra of the metal regions of the sputter profiles shown in Figure 1. (a) Ta film close to the surface indicates Ta^{5+} oxide, while (b) taken near the interface with silicon shows a mixture of Ta^{5+} and Ta^{0}. Similarly, (c) shows the surface niobium is present predominantly as Nb^{5+} oxide, while at the silicon interface (d) it is mainly Nb^{2+} oxide. Results for bismuth oxide indicate Bi^{3+} oxide peaks at the surface (e); elemental bismuth, Bi^{0}, is detected deep in the film (f). Spectra for cerium oxides at the silicon interface (h) is consistent with pure Ce^{3+} oxide, while the overlap of the peaks in (g) indicates the presence of Ce^{4+} oxide at the surface of the film.

to the Si wafer interface the Ta^{5+} oxide peaks are less intense and peaks at 22.6 eV ($4f_{7/2}$) emerged, suggesting that Ta^{0} is also present.[34] A similar result is observed for bismuth where Bi^{3+} oxide at the surface of the film is indicated by peaks at 164 eV ($4f_{5/2}$) and 159 eV ($4f_{7/2}$), Figure 5e. Closer to the Si wafer interface, peaks at 162 eV ($4f_{5/2}$) and

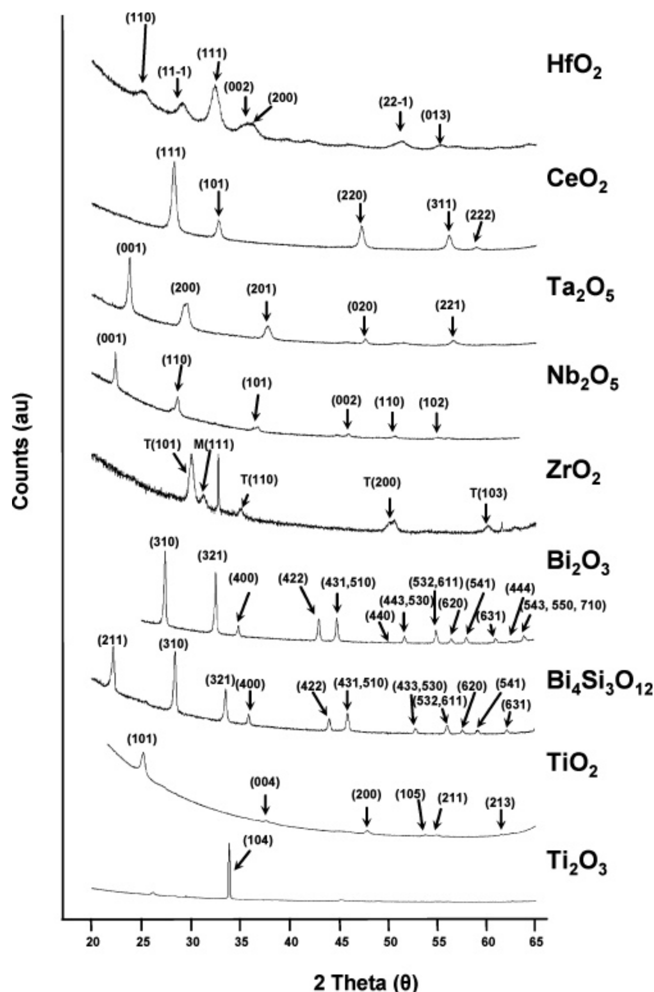

Figure 6. XRD data for oxide films following an 800 °C anneal. All films were annealed over 6 h, except for TiO_2 and Bi_2O_3, which were annealed for 1 h. After 6 h these systems formed Ti_2O_3 and $Bi_4Si_3O_{12}$, respectively (see text).

157 eV ($4f_{7/2}$) appeared, which are indicative of the zero oxidation state of bismuth, Figure 5f. Niobium oxide films also contain mixed oxidation states, Figures 5c and 5d. Surface peaks at 211.2 eV ($3d_{3/2}$) and 208.3 eV ($3d_{5/2}$) indicate Nb^{5+} oxide, while at the interface peaks at 204.0 eV ($3d_{3/2}$) and 206.3 eV ($3d_{5/2}$) indicate the presence of Nb^{2+} oxide.[34]

XRD analysis indicated that the as-deposited films were amorphous in all cases. Annealing at 800 °C for 1 and 6 h in air induced significant crystallization in all the films with the exception of ceria (Figure 6). The XRD patterns generally exhibited broad peaks, indicating small crystallites. In some cases small crystallites gave rise to extremely broad peaks, making indexing difficult. HfO_2 is one such case where the observed pattern fits known data; however, indexing of the peaks was not possible.[35,36] CeO_2 appears to be the dominant crystalline species in the diffraction pattern of the annealed ceria films, as is consistent with results for films deposited by other techniques.[37] Given that the XPS results indicate that the films deposited in this study are primarily Ce_2O_3 both prior to and after annealing, the XRD results suggest the majority of the film remains amorphous after the annealing step. The CeO_2 pattern shown in Figure 6 indexes to a cubic fluorite structure $a = 5.4034$ Å (published value $a = 5.4110$ Å).[36,38] Ta_2O_5 is consistent with the orthorhombic (β) form as described by Joshi and others.[39,40] The result for Nb_2O_5 similarly is consistent with published structures.[41,42] ZrO_2 peaks are broader and are consistent with a mixture of ZrO_2 in the common monoclinic and metastable tetragonal forms.[43−45] Increasing the annealing time to 6 h increased the relative intensity of diffraction peaks in the Ta_2O_5, Nb_2O_5, HfO_2, Ce_2O_3, and ZrO_2 cases. Longer annealing led to the formation of new diffraction patterns in the cases of bismuth and titanium. For bismuth the formation of a silicate structure is due to the high mobility of the bismuth at high temperatures and is consistent with the XPS data shown above. The bismuth oxide film annealed for 1 h indexes to a cubic lattice, $a = 10.2854$ Å, of the gamma polymorph of Bi_2O_3 (reported value $a = 10.2500$ Å).[36] On further annealing a different cubic lattice structure emerges, $a = 10.2697$ Å, which fits data for the $Bi_4Si_3O_{12}$ lattice (reported value $a = 10.3000$ Å).[36,46] TiO_2 crystallized purely in the anatase[36] form when annealed for 1 h but on further annealing yields Ti_2O_3.[47] No peaks consistent with the rutile form were observed. No attempt was made to optimize the annealing conditions and future work will be directed toward reducing annealing temperatures.

Conclusion

Deposition of high-purity conformal metal oxide films has been demonstrated by supercritical fluid deposition. These films generally contain $<5\%$ carbon on deposition, which can be removed with a 400 °C anneal. High temperature is required to initiate formation of the crystalline phase and reduce or eliminate instances of mixed oxidation states for Ce, Bi, Ta, and Nb oxides. Conformal coverage within high aspect ratio features has been demonstrated for these systems. Depositions of many other oxide and mixed oxide films are certainly possible and would be facilitated by the development of additional $scCO_2$ soluble precursors.

(34) Moulder, J. E.; Stickle, W. F.; Sobol, P. E.; Bomben, K. P. *Handbook of X-Ray Photoelectron Spectroscopy*; Physical Electronics Inc.: Chanhassen: MN, 1995.
(35) Kim, S. K.; Ko, Y. D.; Yun, M.; Hong, J. H.; Jeong, M. C.; Myoung, J. M.; Yun, I. *Mater. Sci. Eng., B* **2005**, *123*, 20−30.
(36) www-mincryst; http://database.iem.ac.ru/mincryst/; accessed Jan 2006.
(37) Logothetidis, S.; Patsalas, P.; Charitidis, C. *Mater. Sci. Eng., C* **2003**, *23*, 803−806.
(38) Wyckoff, R. W. G. *Crystal Structures*, 2nd ed.; Interscience Publishers: New York, 1963; Vol. 1, pp 8−11.
(39) Joshi, P. C.; Cole, M. W. *J. Appl. Phys.* **1999**, *86*, 871−880.
(40) Roth, R. S.; Waring, J. L.; Parker, H. S. *J. Solid State Chem.* **1970**, *2*, 445.
(41) Witkowski, S.; Ruszak, M.; Sayag, C.; Pielaszek, J.; Djega-Mariadassou, G. *Appl. Catal., A* **2006**, *307*, 205−211.
(42) Kominami, H.; Oki, K.; Kohno, M.; Onoue, S.; Kera, Y.; Ohtani, B. *J. Mater. Chem.* **2001**, *11*, 604−609.
(43) Gao, Y.; Masuda, Y.; Ohta, H.; Koumoto, K. *Chem. Mater.* **2004**, *16*, 2615−2622.
(44) Kukli, K.; Ritala, M.; Matero, R.; Leskela, M. *J. Cryst. Growth* **2000**, *212*, 459−468.
(45) Lin, J. M.; Hsu, M. C.; Fung, K. Z. *J. Power Sources* **2006**, *159*, 49−54.
(46) Rico-Fuentes, O.; Sanchez-Aguilera, E.; Velasquez, C.; Ortega-Alvarado, R.; Alonso, J. C.; Ortiz, A. *Thin Solid Films* **2005**, *478*, 96−102.
(47) Simcock, M. N. *Surf. Interface Anal.* **2006**, *38*, 1122−1129.

Acknowledgment. We gratefully acknowledge financial assistance from the NSF (CTS-0245002) and the NSF Center for Hierarchical Manufacturing (CMMI-0531171). Instruments supported by the Materials Research Science and Engineering Center at the University of Massachusetts were used for analysis. We acknowledge the assistance of Jack Hirsch and Christos Karanikas with the interpretation of the XPS data.

CM070288S